# Mechanical properties of AlSi10Mg processed by laser powder bed fusion at elevated temperature

Even W. Hovig[1], Amin S. Azar[2], Mohammed Mhamdi[2] and Knut Sørby[1]

**Abstract** AlSi10Mg processed by laser powder bed fusion is expected to have remarkable mechanical properties due to the dominant cellular microstructure. However, the as-processed material is often both anisotropic and containing significant residual stresses. To mitigate these problems, a retrofitted heating system was used to elevate the process temperature to 200°C. The characterization results show low levels of porosity, anisotropy and residual stress. Furthermore, the effect of three heat treatment conditions (as-built, stress relief, and T6) on the tensile properties was investigated. For this purpose, 14 tensile samples were built in seven different orientations. Digital image correlation was used to understand the deformation mechanism for each heat treatment condition. It was observed that the as-built material has comparable properties to the stress relieved condition, while T6 heat treatment resulted in increased ductility. Based on the results, LPBF processing of AlSi10Mg at elevated temperature can potentially eliminate the need for post-process stress relief heat treatment.

**Keywords** Powder bed fusion, Laser melting, Additive manufacturing, Residual stress, Tensile properties, Anisotropy, Digital image correlation.

## 1. Introduction

AlSi10Mg processed by laser powder bed fusion (LPBF) have received significant attention in the scientific community. Challenges with respect to microstructure, heat treatment and anisotropy are still limiting the adaptation in the industry, however [1]. The material is known to have a high degree of residual stresses and anisotropy in the as-built condition [1-5]. T6 heat treatment (solution treatment plus artificial ageing) is known to reduce both the residual stresses and the anisotropy at the cost of strength and hardness, due to the recrystallization and grain growth of the microstructure [2, 5]. Stress relief is another commonly used heat treatment, as suggested by some of the major powder suppliers [6-8], which reduces the residual stresses and leaves the microstructure intact [9].

The effect of (pre-)heating the build platform on the microstructure and mechanical properties of AlSi10Mg and the similar alloy AlSi12Mg have been reported in several studies [10-12]. The main findings suggest that pre-heating the build platform can reduce the quantity and size of internal defects, reduce the residual stresses, and consequently increase the usability of the process and material.

In this work, we cover the microstructure, residual stresses, and tensile properties of AlSi10Mg processed by laser powder bed fusion at elevated bed temperature. To investigate the effect of the elevated temperature on the anisotropy of the material, tensile specimens processed at different orientations are studied.

## 2. Materials and method

### 2.1. Specimen preparation

The AlSi10Mg specimens were prepared by the Concept Laser M2 Cusing machine. The AlSi10Mg powder feedstock was supplied by the machine vendor (CL31Al by Concept Laser). The following processing parameters were used: laser power P = 200 W, laser scan velocity v = 1400 mm/s, layer thickness t = 30 μm, hatch spacing h = 97.5 μm. Prior to the layer fusion, each layer was preheated by a 50 W pre-scan. The build platform was heated from below using a retrofitted heating system to keep the build platform at 200°C throughout the entire process. The employed scan strategy was the 'island' type by Concept Laser, with 2 mm islands with an angular shift of 45° and

an XY-shift of 0.4 mm between each layer. The processing parameters were selected based on a previous study of the same machine and material which resulted in a relative density of 99.90 % [13].

Three sets of 14 rectangular blocks were processed by LPBF at seven different orientations (0° to 90° at 15° increments with respect to the build platform). The blocks were then heat treated before machined to rectangular cross section tensile specimens as shown in Figure 1.a. Two cantilever beams aligned in the X and Y direction of the LPBF machine (Figure 1.b) were manufactured to measure the magnitude of the released residual stresses. An additional set of two cantilever beams were manufactured using a laser scan speed of 1200 mm/s without heating in the build plate, to act as a control for the residual stress investigations.
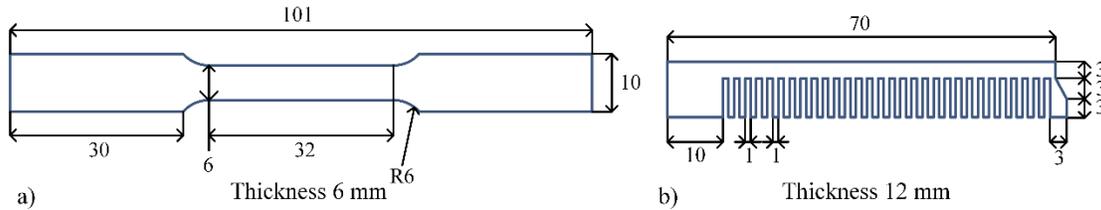


*Figure 1 Dimensions of tensile specimens (a), and cantilever beams (b). All units in mm.*

## 2.2. Heat treatment

Each of the three sets of tensile specimens were subjected to different heat treatments. The first set received no heat treatment (denoted as AB), while the second set was stress relieved at 300°C for 2 hours following air cooling to room temperature (denoted as SR). The last set was solution annealed at 536°C for 2 hours in argon atmosphere followed by water quenching, before an artificial ageing at 160°C for 12 hours followed by air cooling to room temperature (denoted as T6).

## 2.3. Residual stress

To get insight into the residual stresses of the material, the deflection in in Z-direction in the cantilever beams after cutting with wire-EDM was measured with a portable CMM (Leica AT960). The inherent strains and stresses were calculated with the calibration feature in the Simufact Additive 4.0 analysis software using an element size of 0.5 mm and the iterative sparse solver.

## 2.4. Tensile test

The tensile tests were carried out in a Zwick/Roell Z250 with a 50 kN load cell at a displacement rate of 1 mm/min. The displacement field on two perpendicular sides of each specimen was captured with a commercial DIC system (VIC 3D). A detailed description of the DIC system and set-up is given in [14].

## 2.5. Microscopy

For SEM imaging and EDS investigations, the samples were prepared by mechanical grinding and polishing, followed by a single step electropolishing using standard Struers recipe. The microscope is a FEI NOVA NANOSEM 650 ultralow vacuum field emission gun scanning electron microscope (SEM) equipped with an X-Max 50 mm$^2$ EDS detector from Oxford Instruments.

# 3. Results and discussion

## 3.1. Residual stress

The deflection in Z-direction after cutting the cantilever beams processed at 200°C was measured to 0.22 mm and 0.23 mm for the beams aligned with the X and Y direction respectively. The corresponding displacements in the cantilever beams processed at room temperature was measured to 2.723 mm and 2.808 mm. The calibration process in Simufact Additive 4.0 estimates the inherent strains before calculating the displacement after the cutting process. The inherent strains are then changed as the calibration process iterates until the least-squares error is below 3%.

The resulting inherent strains are $\epsilon_x$=-0.00025, $\epsilon_y$=-0.00033 at 200°C and $\epsilon_x$=-0.00458, $\epsilon_y$=-0.00600 at room temperature. Note that the inherent strains are specific to the current process parameters and material. The simulated residual stresses, corresponding to the measured displacement for the two processing conditions, are shown in Figure 2.
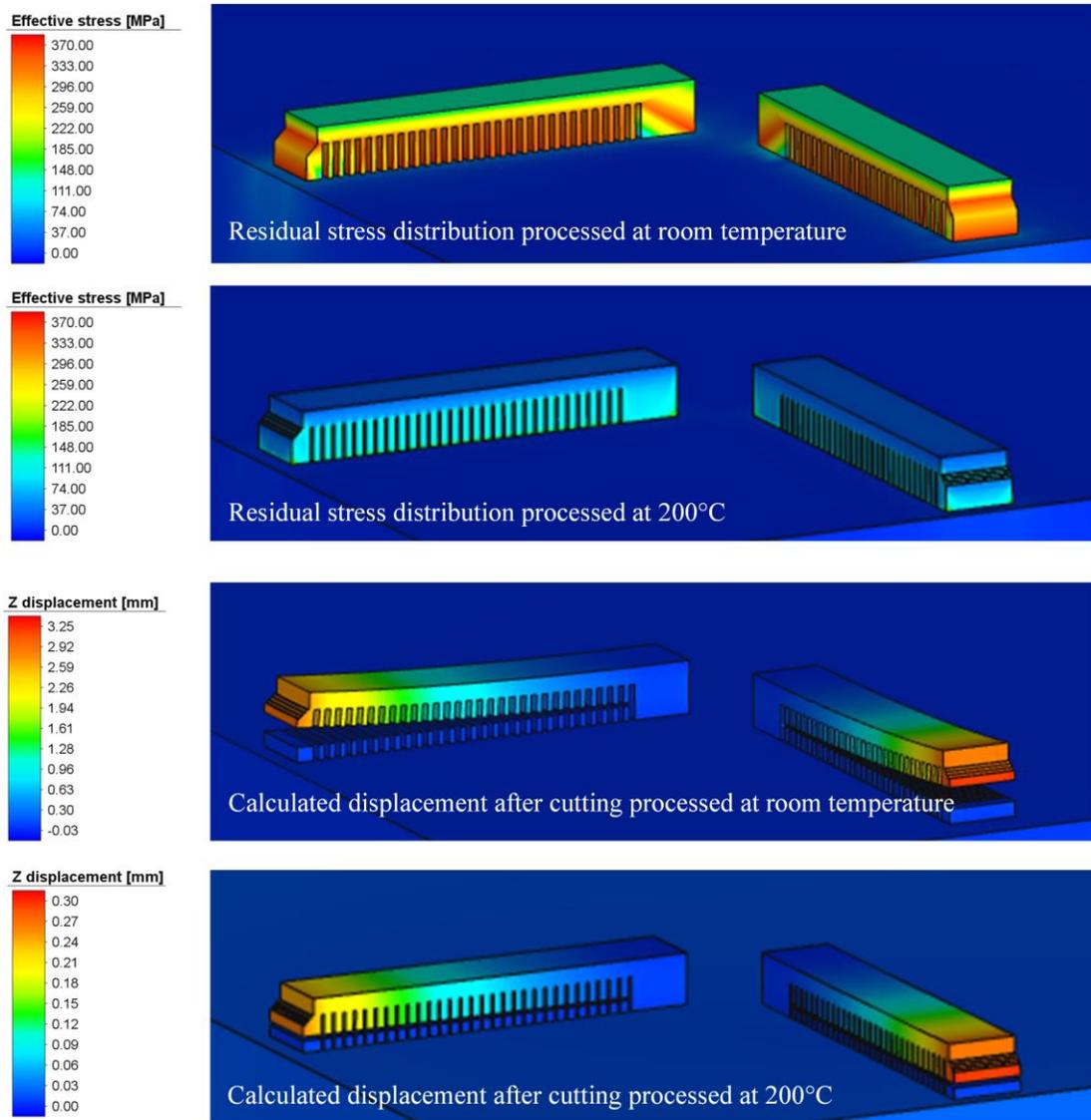


*Figure 2 Residual stress distribution and calculated displacement after cutting for AlSi10Mg processed at room temperature and at 200°C*

The effective stress distribution in the specimens built at 200°C is reduced by approximately 40%, down from a maximum of 370 MPa when processed at room temperature to a maximum of 210 MPa. The reduction of residual stress is attributed to the lower temperature gradient between the melt pool and substrate or previously fused layers, reducing the difference in thermal expansion throughout the component. The indications of the reduced residual stress can be inferred from the displacement after the cantilever beam is cut from its supports. The displacement is calculated based on the inherent strains, which in turn are estimated from the measured displacement. The error between measured displacement and calculated displacement is less than 3% for both processing conditions.

According to simulations by Sehrt et al. [15] a temperature of 300°C is necessary to reduce residual stresses. This is dependent on the remaining parameters, however, and as demonstrated here, 200°C seems sufficient to significantly

reduce the residual stresses with the current process parameters. Bagherifard et al. [2] demonstrates that the laser parameters may be adjusted such that a substrate temperature of 150°C provides a reduction of residual stresses.

## 3.2. Tensile properties

Figure 3 plots the Cauchy stress against the Lagrange strain as calculated based on the DIC displacement fields for all specimens. Details about DIC, Cauchy stress, and Lagrange strain can be found in [14]. As can be seen the AB and SR heat treatment condition behaves similarly with a relatively high yield strength and ultimate tensile strength (UTS), and low elongation at break. As expected, the T6 heat treatment condition increases the elongation at break at the cost of strength.
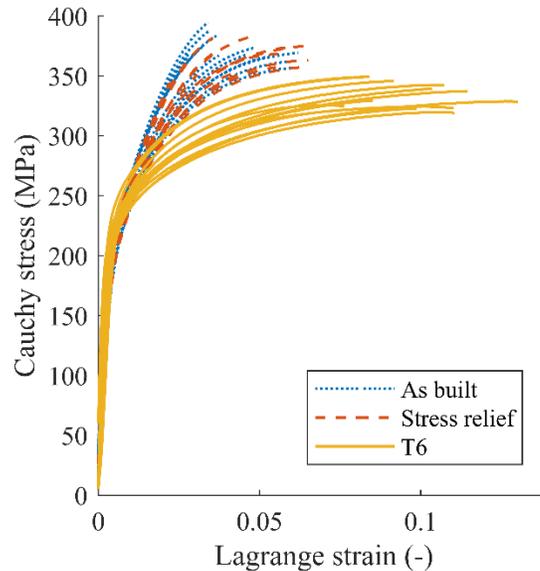


*Figure 3 Cauchy stress plotted against the Lagrange strain for all 14 samples from each of the three heat treatment conditions*

Figure 4 shows selected tensile properties plotted against the build orientation for each specimen. The build orientation does not appear to alter the elastic modulus for the applied heat treatment conditions, although the scatter in the data is substantial. This suggests that the crystallographic texture, if any, has a limited effect on the elastic anisotropy. Hitzler et al. [4] found the elastic modulus to be sensitive to the orientation when processed at elevated temperature, but this is attributed to deviations in their applied laser scan patterns. Tang et al. [3] reports no significant sensitivity in the elastic modulus with respect to orientation, which further suggests that the crystallographic texture is insignificant with respect to anisotropy in the elastic behavior.

The yield strength and UTS appears to take a dip at 15° before steadily increasing as the specimens are raised towards 75° for the T6 heat treatment condition, which can be a result of retained melt pool boundaries even after recrystallization. There is no apparent correlation between build orientation and strength for the AB and SR heat treatment conditions. Interestingly, the elongation at break increases as the specimens are tilted from 0° (parallel to the build-plate) to 90° (perpendicular to the build-plate) in the AB and SR heat treatment conditions. This plastic anisotropy suggests that a crystallographic textured microstructure might influence the failure mode, as observed on e.g. LPBF Inconel 718 by [14, 16]. As the specimens are raised from 0° to 90°, the angle between the load direction and the assumed preferred orientation in the microstructure changes, either promoting or limiting mode I type failure. Another explanation of the plastic anisotropy can be the effect of the melt pool boundaries, and how they align with the load direction, which is discussed in the next section.
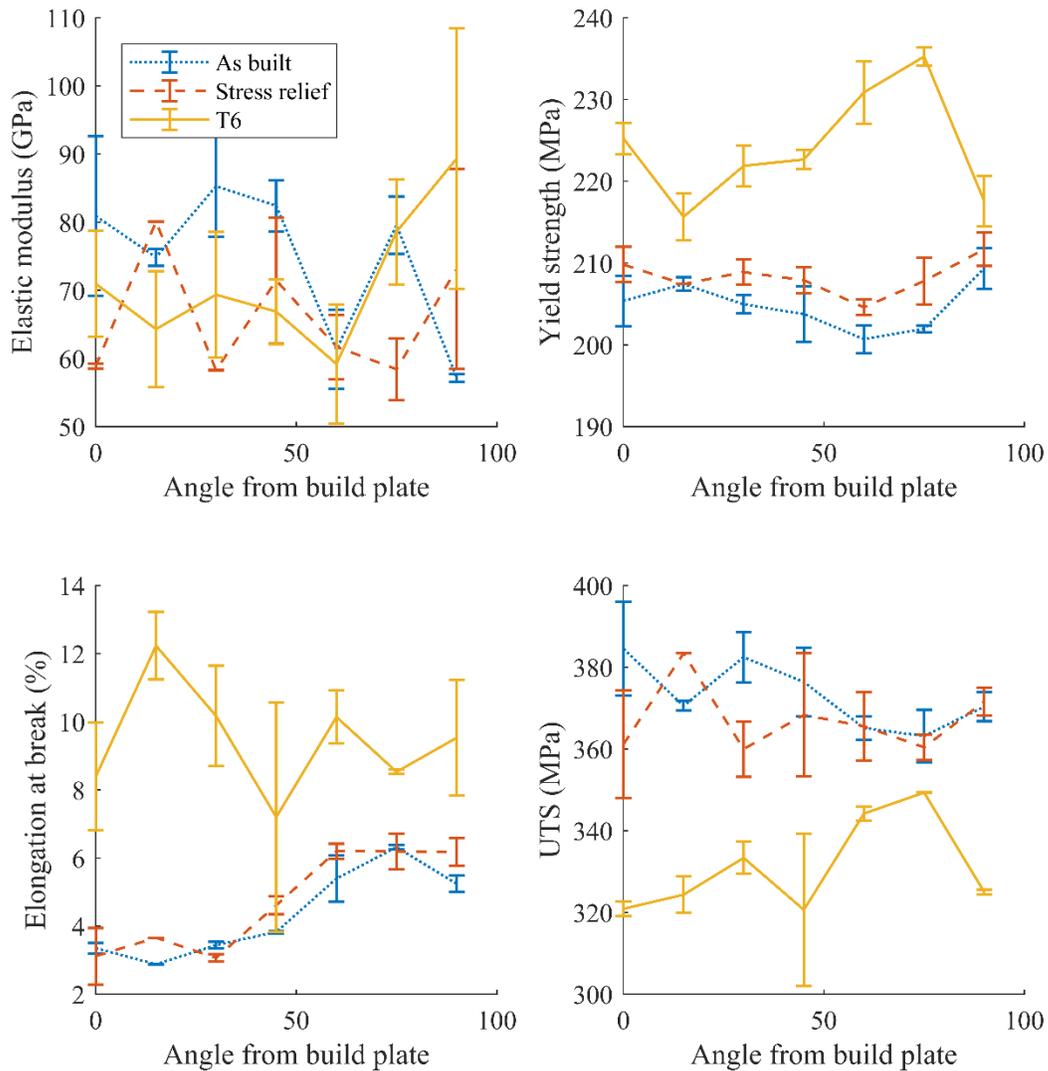
*Figure 4 Tensile properties plotted as a function of specimen orientation with respect to the build platform*

The average tensile properties for each heat treatment condition are listed in Table 1. As mentioned, the AB and SR heat treatment conditions shows no significant difference in tensile properties. This is attributed to the elevated temperature in the build plate during LPBF processing, resulting in a great reduction of residual stresses. Consequently, SR treatment might be considered superfluous, eliminating a step in the process chain. The average elongation at break is doubled after T6 treatment, but the yield strength and UTS is reduced by approximately 10% as compared to AB and SR. Both the elastic and plastic Poison's ratios are slightly reduced in the T6 condition as well. The Poisson's ratio in the elastic region is determined according to ASTM E132-17. The Poisson's ratio in the plastic region is the average of the local Poisson's ratios for each data point for each point above the yield strength (~ 175 points).

*Table 1 Average tensile properties for each heat treatment condition*

| Condition | E (GPa) | Yield (MPa) | UTS (MPa) | ε (%) | $\nu_{elastic}$ (-) | $\bar{\nu}_{plastic}$ (-) |
|---|---|---|---|---|---|---|
| As-built (AB) | 74.5 ± 12.3 | 204.8 ± 3.6 | 373.2 ± 10.4 | 4.35 ± 1.28 | 0.355 ± 0.026 | 0.459 ± 0.006 |
| Stress relieved (SR) | 66.0 ± 11.2 | 208.3 ± 2.8 | 367.2 ± 12.1 | 4.72 ± 1.48 | 0.350 ± 0.029 | 0.459 ± 0.004 |
| T6 | 71.2 ± 14.3 | 224.2 ± 7.2 | 331.1 ± 13.56 | 9.46 ± 2.36 | 0.343 ± 0.041 | 0.437 ± 0.014 |

## 3.3. Microstructural investigations

Figure 6 shows SEM images of the loaded cross section at low magnification for AB and T6 heat treatment at 0°, 45°, and 90° orientation. The T6 heat treatment (d-f) mostly homogenizes the microstructure and removes the melt pool boundaries which are clearly visible in the AB condition (a-c).
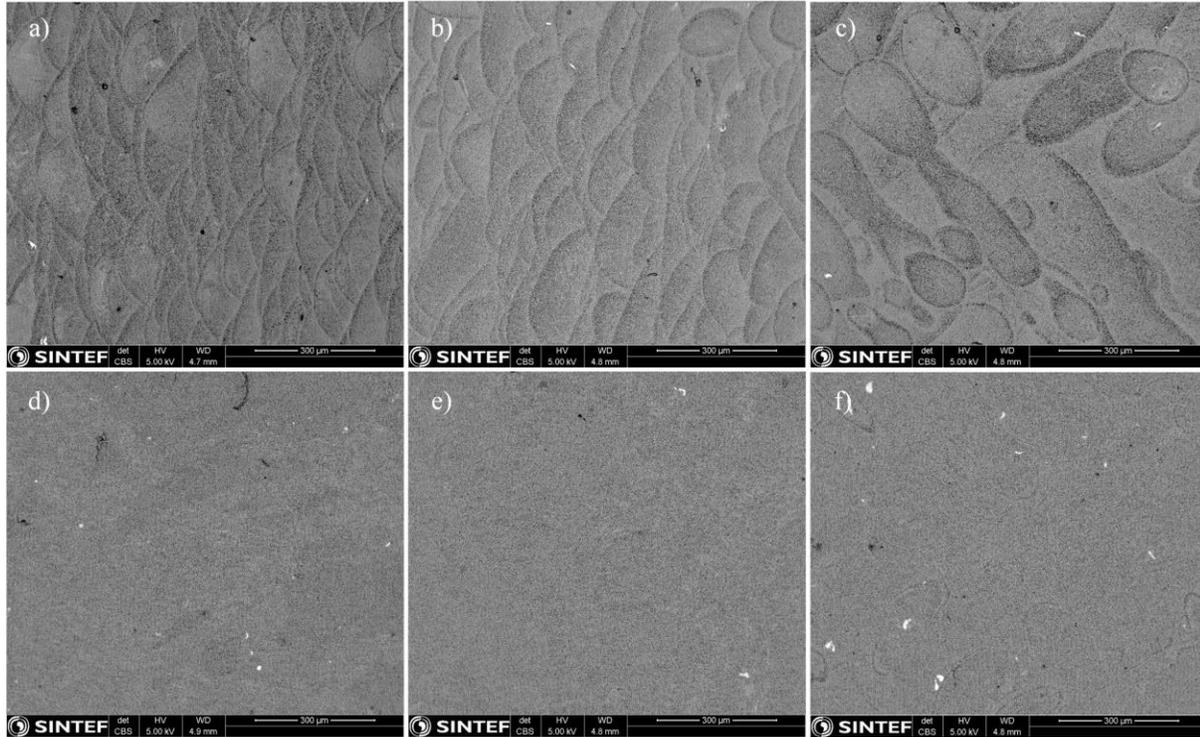


*Figure 5 SEM images of a) AB 0°, b) AB 45°, c) AB 90°, d) T6 0°, e) T6 45°, f) T6 90°*

In the as-built condition the microstructure is fine-grained with a cellular-dendritic structure, with Si-rich cell-boundaries (Figure 6.a). During T6 heat treatment the microstructure is recrystallized, and the eutectic Si structure formed spheroidized particles during the artificial ageing (Figure 6.b and c). The findings are comparable to [2, 17] where the LPBF specimens were processed both at room temperature and at elevated temperature. Bagherifard et al. reports that the grain size is finer in the melt pool and coarser on the boundary of the melt pool only when processing at room temperature [2]. The complete homogenization of the microstructure observed by [2] when processing at elevated temperature is not observed in this study. As can be seen in Figure 6.a, the microstructure is still coarser at the right-hand side of the image, corresponding to the boundary of the melt pool. Brandl et al. [17] also reports a slightly inhomogeneous microstructure even when processed at 300°C. According to Xiong et al. [18] anisotropic tensile properties is driven by the distribution of the melt pool boundaries on the load bearing cross section, irrespective to the microstructural texture. Even though the melt pool boundaries in the AB condition is clearly visible, no definitive elastic anisotropy is observed in this study. The elongation at break indicates plastic anisotropy, which as mentioned can be attributed to the melt pool boundaries observed in the AB condition Figure 5.a-c.
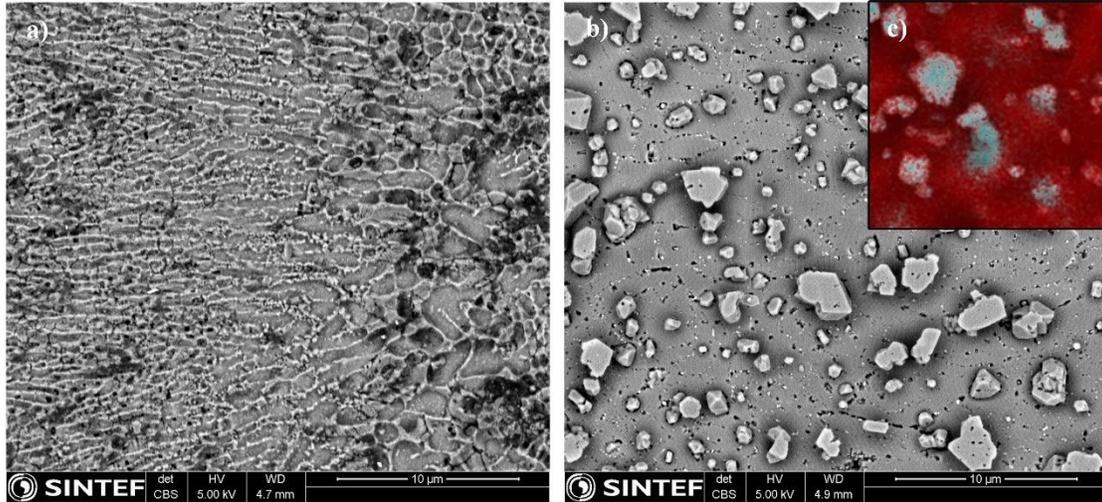
*Figure 6 SEM images of a) as-built heat treatment condition - 0° specimen, b) T6 heat treatment condition - 0° specimen, c) EDS map of Al (red) and Si (cyan) of the T6 condition (same scale).*

## 4. Summary and conclusions

This study demonstrates the effect of elevating the build plate temperature during LPBF processing of AlSi10Mg on the build stresses, tensile properties, and microstructure. Elevating the build plate temperature have several positive effects, such as:

- An estimated reduction in the effective residual stress by approximately 40%.
- Potentially eliminating the need for SR treatment of AlSi10Mg components processed by LPBF. For parts where toughness is considered more important than strength, T6 heat treatment can increase the ductility at the cost of a reduction in strength.
- Any crystallographic texture appears to be insignificant in the elastic part of the flow curve, as there is no apparent relationship between elastic modulus and build orientation. In a future work the material should be investigated with EBSD to get a better understanding of the (preferred) grain orientation.

The elongation at break in the AB and SR condition is linearly dependent on build orientation. Specimens built parallel to the build plate exhibits the lowest elongation at break. The recrystallization of the microstructure after T6 heat treatment eliminates the sensitivity to build orientation and effectively doubles the elongation at break, at the cost of a slight reduction in strength.

**References**

[1] F. Trevisan, F. Calignano, M. Lorusso, J. Pakkanen, A. Aversa, E. Ambrosio, M. Lombardi, P. Fino, D. Manfredi, On the Selective Laser Melting (SLM) of the AlSi10Mg Alloy: Process, Microstructure, and Mechanical Properties, Materials 10(1) (2017) 76.

[2] S. Bagherifard, N. Beretta, S. Monti, M. Riccio, M. Bandini, M. Guagliano, On the fatigue strength enhancement of additive manufactured AlSi10Mg parts by mechanical and thermal post-processing, Materials & Design 145 (2018) 28-41.

[3] M. Tang, P.C. Pistorius, Anisotropic Mechanical Behavior of AlSi10Mg Parts Produced by Selective Laser Melting, JOM 69(3) (2017) 516-522.

[4] L. Hitzler, C. Janousch, J. Schanz, M. Merkel, B. Heine, F. Mack, W. Hall, A. Öchsner, Direction and location dependency of selective laser melted AlSi10Mg specimens, Journal of Materials Processing Technology 243 (2017) 48-61.

[5] P. Yang, M.A. Rodriguez, L. Deibler, B. Jared, J. Griego, A. Kilgo, A. Allen, D. Stefan, Effect of thermal annealing on microstructure evolution and mechanical behavior of an additive manufactured AlSi10Mg part, J. Mater. Res. 33(12) (2018) 1701-1712.

[6] Renishaw plc., Data sheet: AlSi10Mg-0403 (200 W) powder for additive manufacturing, 2019. https://resources.renishaw.com/en/details/data-sheet-alsi10mg-0403-200-w-powder-for-additive-manufacturing--73121. (Accessed Aug. 20 2019).

[7] EOS GmbH, EOS Aluminium AlSi10Mg, 2019. https://cdn0.scrvt.com/eos/f3f4bf485d78f2dd/b010c05abe97/AlSi10Mg-090-M400_Flexline_Material_data_sheet_09-15_en.pdf. (Accessed Aug 20. 2019).

[8] edmit inc., Material Data Sheet CL 30AL / CL 31AL Aluminium alloy, 2019. http://edmitinc.com/download/EDMIT_ALUMINUM_AlSi12_AlSi10Mg.pdf. (Accessed 20 Aug 2019).

[9] N.E. Uzan, R. Shneck, O. Yeheskel, N. Frage, Fatigue of AlSi10Mg specimens fabricated by additive manufacturing selective laser melting (AM-SLM), Materials Science & Engineering A 704 (2017) 229-237.

[10] E.W. Hovig, H.D. Holm, K. Sørby, Effect of Processing Parameters on the Relative Density of AlSi10Mg Processed by Laser Powder Bed Fusion, Springer Singapore, Singapore, 2019, pp. 268-276.

[11] S. Siddique, M. Imran, E. Wycisk, C. Emmelmann, F. Walther, Influence of process-induced microstructure and imperfections on mechanical properties of AlSi12 processed by selective laser melting, Journal of Materials Processing Technology 221 (2015) 205-213.

[12] S. Romano, A. Brückner-Foit, A. Brandão, J. Gumpinger, T. Ghidini, S. Beretta, Fatigue properties of AlSi10Mg obtained by additive manufacturing: Defect-based modelling and prediction of fatigue strength, Engineering Fracture Mechanics 187 (2018) 165-189.

[13] M. Reiersen, Microstructural Analysis of SLM AlSi10Mg and Al7075 Alloys - Topology Optimisation in Redesigning Novel Parts to be Produced by SLM, Department of Chemistry, University of Oslo, 2019.

[14] E.W. Hovig, A. S. Azar, F. Grytten, K. Sørby, E. Andreassen, Determination of Anisotropic Mechanical Properties for Materials Processed by Laser Powder Bed Fusion, Adv. Mater. Sci. Eng. (2019).

[15] J.T. Sehrt, G. Witt, B. Müller, T. Töppel, K.P.J. Hoeren, B. Reinarz, Less residual stresses in laser beam melting by investigating on supports, powder layer properties, powder preheating and scanning strategies: Presentation held at International Symposium on Additive Manufacturing, February 25th-26th, 2015, Dresden; ISAM 2015, 2015.

[16] M. Ni, C. Chen, X. Wang, P. Wang, R. Li, X. Zhang, K. Zhou, Anisotropic tensile behavior of in situ precipitation strengthened Inconel 718 fabricated by additive manufacturing, Materials Science and Engineering: A 701 (2017) 344-351.

[17] E. Brandl, U. Heckenberger, V. Holzinger, D. Buchbinder, Additive manufactured AlSi10Mg samples using Selective Laser Melting (SLM): Microstructure, high cycle fatigue, and fracture behavior, Materials & Design 34 (2012) 159-169.

[18] Z.H. Xiong, S.L. Liu, S.F. Li, Y. Shi, Y.F. Yang, R.D.K. Misra, Role of melt pool boundary condition in determining the mechanical properties of selective laser melting AlSi10Mg alloy, Materials Science and Engineering: A 740-741 (2019) 148-156.